AIP | Applied Physics Letters

# Room temperature negative differential resistance in terahertz quantum cascade laser structures

Asaf Albo, Qing Hu, and John L. Reno

Citation: Applied Physics Letters **109**, 081102 (2016); doi: 10.1063/1.4961617
View online: http://dx.doi.org/10.1063/1.4961617
View Table of Contents: http://scitation.aip.org/content/aip/journal/apl/109/8?ver=pdfcov
Published by the AIP Publishing



# Room temperature negative differential resistance in terahertz quantum cascade laser structures

Asaf Albo,[1,a)] Qing Hu,[1] and John L. Reno[2]
[1]*Department of Electrical Engineering and Computer Science and Research Laboratory of Electronics, Massachusetts Institute of Technology, Cambridge, Massachusetts 02139, USA*
[2]*Center for Integrated Nanotechnologies, Sandia National Laboratories, MS 1303, Albuquerque, New Mexico 87185-1303, USA*

(Received 16 June 2016; accepted 7 August 2016; published online 24 August 2016)

The mechanisms that limit the temperature performance of GaAs/$Al_{0.15}$GaAs-based terahertz quantum cascade lasers (THz-QCLs) have been identified as thermally activated LO-phonon scattering and leakage of charge carriers into the continuum. Consequently, the combination of highly diagonal optical transition and higher barriers should significantly reduce the adverse effects of both mechanisms and lead to improved temperature performance. Here, we study the temperature performance of highly diagonal THz-QCLs with high barriers. Our analysis uncovers an additional leakage channel which is the thermal excitation of carriers into bounded higher energy levels, rather than the escape into the continuum. Based on this understanding, we have designed a structure with an increased intersubband spacing between the upper lasing level and excited states in a highly diagonal THz-QCL, which exhibits negative differential resistance even at room temperature. This result is a strong evidence for the effective suppression of the aforementioned leakage channel. *Published by AIP Publishing.* [http://dx.doi.org/10.1063/1.4961617]

The maximum operating temperature ($T_{max}$) reported so far for pulsed operations of terahertz quantum cascade lasers (THz-QCLs) is ~200 K.[1] This record operating temperature is achieved based on an extensively developed GaAs/$Al_{0.15}$GaAs material system. One straightforward strategy to further improve their temperature performance is by reducing the thermally activated LO-phonon (TA-LOP) scattering rate by using structures with highly diagonal optical transition.[2] However, the effectiveness of this method for achieving $T_{max}$ values significantly higher than ~200 K remains to be demonstrated. In a recent study, the reason for the lack of improvement is suggested to be the thermally activated leakage of carriers into the continuum (TA-LTC).[3] Based on this study, barriers higher than 15% aluminum concentration would be beneficial to reduce this leakage channel.[4–6] Going forward, the combination of highly diagonal structures and higher barriers should significantly reduce both the TA-LOP scattering and TA-LTC.[3]

This expected behavior is illustrated in Figure 1 with the calculations of output power dependence on temperature for a highly diagonal THz-QCL in the two limiting cases of including or excluding the TA-LTC, respectively. These calculations show that an effective suppression of the TA-LTC in highly diagonal structures (in which the only temperature dependent mechanism is the TA-LOP scattering from the upper to lower lasing levels, ULL and LLL, respectively) should result in a much higher $T_{max}$ value. However, despite the expectation for a major breakthrough by reducing the TA-LTC, to-date no significant improvement in temperature performance has been achieved by increasing the barriers height in THz-QCL devices.[4–6]

Here, motivated by this inconsistency between the theoretical expectations and the actual performance of high-barrier devices, we study highly diagonal GaAs/$Al_{0.30}$GaAs-based THz-QCLs and analyze the physical mechanisms that affect their temperature performance. Based on the analysis, we designed a new THz-QCL structure with low leakage at room temperature as manifested by the measured negative differential resistance (NDR). This encouraging result suggests the suppression of various leakage channels remains effective even at room temperature, which clearly is a necessary condition to achieve lasing at that temperature.

We started our analysis with a highly diagonal resonant-phonon THz-QCL with an oscillator strength of $f \sim 0.2$ based on the GaAs/$Al_{0.3}Ga_{0.7}$As materials (device HBD, design

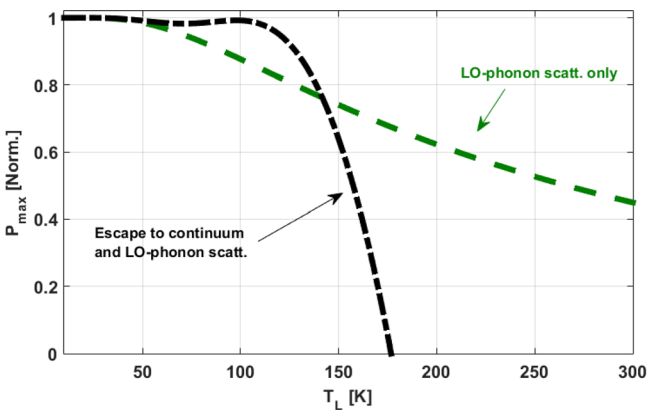


FIG. 1. Calculated normalized photon flux as a function of temperature for a highly diagonal THz-QCL with an oscillator strength of $f \sim 0.2$ and with standard GaAs/$Al_{0.15}$GaAs$_{0.85}$ materials. The black dashed-dotted line marks the calculations including the TA-LTC from both the LLL and ULL, respectively, and TA-LOP scattering from the ULL to LLL. The green dashed line presents the calculation only including the TA-LOP scattering from the ULL to LLL. Further details of the calculation model including the TA-LTC channel are being prepared for publication.[7]

a)asafalbo@gmail.com

TABLE I. Main design parameters and device data.

| Device | Design name (wafer number) | Lasing energy (meV) | $E_{21}$ (meV) | Oscillator strength | Expected activation energy (meV) for TA-LOP scattering | Layer sequence [#ML], barrier composition and doping level | Process details[a] |
|---|---|---|---|---|---|---|---|
| LBD | OWI210H-M3 (VB0605) | 16 | 39 | 0.2 | 20 | **19.8**/29.5/**12.8**/30.5/**16.6**/57.6 210 periods GaAs/**$Al_{0.15}Ga_{0.85}As$** $1.24 \times 10^{17}$ $cm^{-3}$ in the center 17 ML of the 57.6 ML well. | MM(100 Å Ta/2500 Å Au and 100 Å Ta/2500 Å Au) top contact $n^+$ layer was removed dry etched. |
| HBD | OWI213K-M2 (VB0676) | 16 | 35 | 0.2 | 20 | **10.3**/37.2/**6.4**/38.6/**8.2**/65.9 213 periods GaAs/**$Al_{0.3}Ga_{0.7}As$** $1.24 \times 10^{17}$ $cm^{-3}$ in the center 17 ML of the 65.9 ML well. | MM (50 Å Ti/3000 Å Au and 50 Å Ti/3000 Å Au) top contact $n^+$ layer was removed dry etched. |
| VB0743 | OWI258K-M5 (VB0743) | 16 | 55 | 0.2 | 20 | **13.5**/28.3/**8.1**/26.9/**12.0**/49.0 258 periods GaAs/**$Al_{0.3}Ga_{0.7}As$** $1.24 \times 10^{17}$ $cm^{-3}$ in the centered 17 ML of the 49.0 ML well. | MM (100 Å Ta/2000 Å Au/300 Å Ta/ 3000 Å Cu and 100 Å Ta/ 2500 Å Au) top contact $n^+$ layer was removed dry etched. |

[a]In the process details column: the MM stands for metal-metal waveguide, where in the flowing brackets are the metal sequence used for the bottom and top metallization, respectively. In the lower line, the type of etching method used in the process is mentioned. In the layer sequence column, the #ML stand for number of monolayers, where the AlGaAs barriers in **bold** and the GaAs wells in roman, the doped layer in the sequence is underscored and the barriers' composition and doping details are elaborated in the following lines.

OWI213K-M2 and MBE wafer VB0676) and compare its temperature sensitive characteristics with those of a reference structure based on GaAs/$Al_{0.15}Ga_{0.85}As$ materials (device LBD, design OWI210H-M3 and MBE wafer VB0605[3,8]). Device HBD is designed to have similar parameters (lasing frequency, oscillator strength, subband separations, and intersubband LO-phonon scattering times) as device LBD but with higher barriers. The notation "D" in the devices' name stands for "diagonal" design and the notations "LB" and "HB" stand for "low barriers" or "high barriers," respectively, i.e., barriers with the standard composition of 15% aluminum or with a higher one (30% aluminum). More details on these devices are summarized in Tables I and II.

The band structure, pulsed light-current (L-I) measurements, and lasing spectra of devices HBD and LBD are shown in Figure 2. Both devices have similar lasing frequencies around ~4 THz. As evidenced from the experimental data, contrary to the expectation, $T_{max}$ did not improve significantly by increasing the barriers' height. In order to understand this behavior, we analyze in-depth the measured characteristics of device HBD, i.e., I–V curves at different temperatures, the dependence of threshold current density on temperature, and the output power dependence on temperature, and compared them to those of device LBD. Results are presented in Figure 3.

The measured I–V curves at low-temperature of devices HBD and LBD (Figure 3(a)) show typical characteristics for resonant-phonon THz-QCL structures with a pronounced NDR region near the bias where the maximum output power is achieved. The NDR occurs when the preceding module injector level 1′ is raised above the upper lasing level 4. Beyond the NDR region, the current increases again with the bias voltage resulting in a change to positive conductance. The onset of the positive conductance is attributed to TA-LTC that increases exponentially with voltage due to the effect of barrier lowering, as discussed in detail in Ref. 3. From the comparison of the low-temperature I–V curves of devices HBD and LBD, we see that the onset voltage of the NDR region is approximately the same for both samples as expected since the 1′-4 alignment should be approximately the same for these similar designs. However, the onset voltage of the positive conductance beyond NDR shifts to much higher biases for sample HBD, which indicates the extra suppression of the TA-LTC by the increased barrier heights. In addition, Figure 3(a) includes calculations of the leakage current for devices HBD and LBD, which were conducted following Ref. 3. The calculations for device HBD present a correlation with measurements using an increased escape-barrier height of ~265 meV (at zero bias) instead of ~140 meV that is used for device LBD as in Ref. 3.

Figure 3(b) shows the temperature dependence of the threshold current density ($J_{th}$). For the low barrier structure LBD, an exponential behavior occurs only at temperatures not too close to $T_{max}$, with $T_o \approx 105$ K, whereas at temperatures

TABLE II. Device parameters and performance.

| Device | Design name (wafer number) | Injection coupling ($2\hbar\Omega_{ij}$)(meV) | Extraction coupling ($2\hbar\Omega_{ij}$)(meV) | Design electric field (kV/cm) | $\tau^0_{ul}$ (ps)[a] | Lasing energy (meV) | $J_{th}$ (10 K) ($A/cm^2$) | $J_{max}$ (10 K) ($A/cm^2$) | Dynamic range (10 K) ($A/cm^2$) | $T_{max}$ (K) |
|---|---|---|---|---|---|---|---|---|---|---|
| LBD | OWI210H-M3(VB0605) | 1.56 | 3.67 | 12.7 | 1.88 | 16–17 | 246 | 825 | 579 | 177 |
| HBD | OWI213K-M2(VB0676) | 1.77 | 4.29 | 12.0 | 2.11 | 16–17 | 457 | 851 | 394 | 150 |
| VB0743 | OWI258K-M5(VB0743) | 1.83 | 4.36 | 19.7 | 1.79 | 16–17 | 725 | 897 | 172 | 89 |

[a]ULL to LLL raw LO-phonon scattering time.

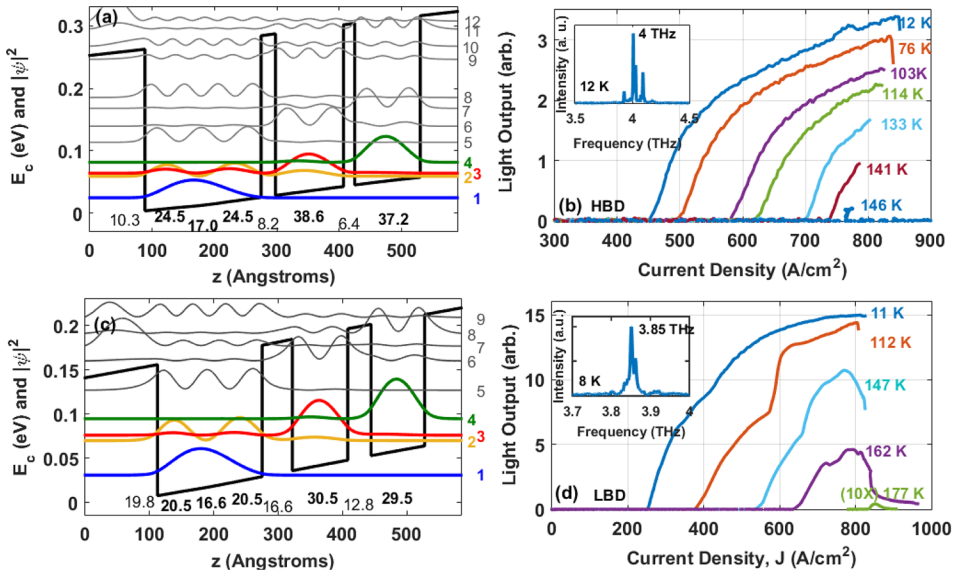


FIG. 2. (a) Band diagram and (b) pulsed light-current measurements for device HBD (VB0676) with its lasing spectra (inset). (c) Band diagram and (d) pulsed light-current measurements for device LBD (VB0605) with its lasing spectra (inset).

near $T_{max}$ a super-exponential rise is observed and $J_{th}$ increases sharply. This super-exponential increase in the threshold current density suggests the onset of the TA-LTC process.[3] For the high-barrier device HBD; however, $J_{th}$ increases exponentially all the way up to $T_{max}$ and its behavior can be well characterized by the phenomenological formula $J_{th}(T) = J_o e^{T/To}$ with $T_o \approx 162$ K. This is another evidence indicating the elimination of the TA-LTC by the increased barrier heights over the studied temperatures range.

These results indicate that the TA-LTC is effectively eliminated in the high-barrier device HBD, which further highlights the inconsistency with the theoretical expectation of a significant improvement in $T_{max}$. To address this issue we took a closer look at the I–V curves in Figure 3(a). We observe that the NDR in the I–V curves gradually disappears with an increased temperature. This behavior implies that there are still thermally activated leakage paths. One possibility is the excitation of carriers into higher energy states. Such thermally activated excitation of carriers followed by their relaxation in non-lasing paths will effectively reduce the upper-state lifetime. Similarly to what happens with TA-LTC, this mechanism will result in a reduced $T_{max}$. A similar phenomenon has been observed in mid-IR QCLs.[9–11] We further test this hypothesis by analyzing the temperature dependence of the output power using the method presented in Ref. 12.

The normalized maximum output power dependence on temperature is presented in Figure 3(c). The output power of device HBD starts to decrease at low temperatures around 40 K and deteriorates at a relatively moderate rate, as predicted by the thermally activated LO-phonon relaxation mechanism (Figure 1). However, as the temperature increases, a sudden drop occurs for the output power around ~130 K. The dotted line in Figure 3(c) illustrates the expected behavior without this sudden drop. In clear contrast, the output intensity of device LBD remains somewhat constant up to ~120 K and drops sharply in a similar manner to device HBD.

Figure 3(d) shows the best fit to the data using Arrhenius plots according to $\ln\left(1 - \frac{P_{out}(T)}{P_{outmax}}\right) \approx \ln(a) - \frac{E_a}{kT}$,

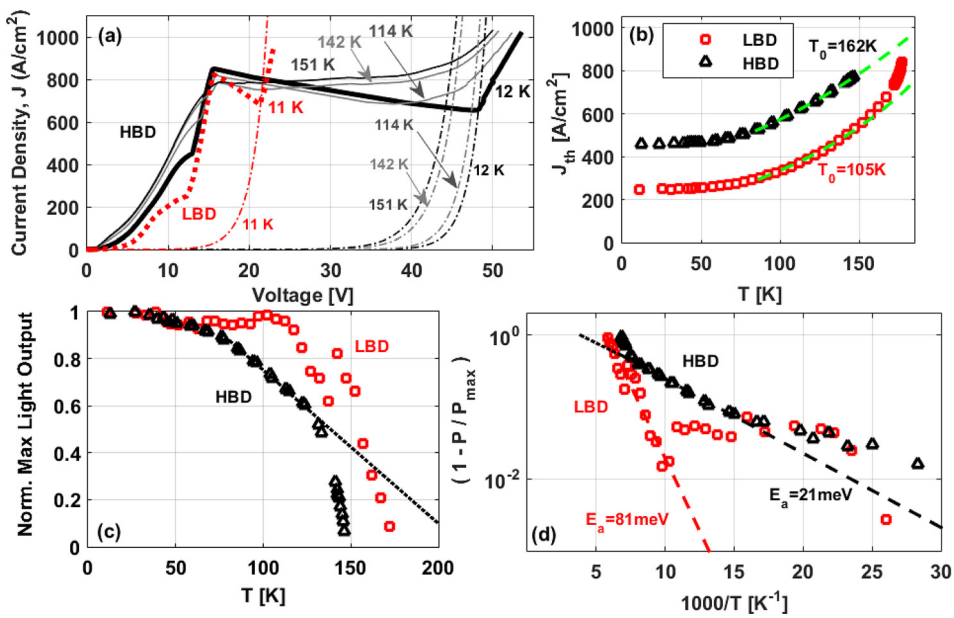


FIG. 3. (a) Measured current–voltage curves at different temperatures of devices HBD (black scale, solid lines) and device LBD (red, dotted line) together with leakage over the barrier calculated following Ref. 3 (dashed-dotted lines). The measurements at the lowest temperature are highlighted by thicker lines. (b) Measured threshold current densities versus temperature with $T_0$ values. The data are shown with red squares for device LBD and black triangles for device HBD. The dashed lines mark the data for $T_0$ extraction with extrapolation to higher temperatures. (c) Normalized output light intensity versus temperature and (d) semi-logarithmic plots of $\left(1 - \frac{P_{out}(T)}{P_{outmax}}\right)$ with fittings (dashed lines) and activation energy values for devices LBD (red squares) and HBD (black triangles), respectively.

where $P_{out}$ is the output power and $a$ is a constant (Ref. 12). A clear difference is observed between the devices HBD and LBD. The activation energy of device LBD, ~80 meV, suggests that thermal excitation of carriers occurs for states located energetically around the barriers' heights.[3] In contrast, device HBD shows a twofold behavior, starting at low temperatures with an activation energy of ~20 meV (which is an indication for TA-LOP relaxation[12]) and followed by a change in mechanism at higher temperatures to a higher value of 82 ± 25 meV, similar to that of device LBD, which is likely associated with the thermal excitation of carriers from level 4 (the ULL) to level 6 in Figure 2(a). The dotted line in the figure illustrates the expected behavior for TA-LOP relaxation only. These characteristics support our interpretation that at high temperatures the thermal excitation of carriers to higher lying levels followed with their relaxation back in non lasing paths is the limiting mechanism in device HBD. This also explains why no improvement occurred in $T_{max}$, although the barrier heights were significantly increased.

To test this interpretation experimentally, we designed a high-barrier structure that is similar to device HBD but with thinner wells (device VB0743 in Table I) so that excited states are pushed towards higher energies. The band structure of this device is presented in Figure 4. In this new structure, the intersubband energy spacing between the ULL and the first (relevant) excited state is increased to ~100 meV (from values around ~60 meV for HBD), As a result of the thinner wells, the energy separation between the LLL-doublet and the injector state is increased to ~55 meV (from the usual value of ~36 meV). Consequently, the design bias in this structure is increased to ~75 mV/module (from the usual ~57 mV/module, which is approximately the sum of the photon and LO-phonon energy divided by $e$).

The I–V curves of this device are presented in Figure 5 at low temperature ~10 K and at room temperature ~290 K along with the data for devices LBD and HBD. The main distinctive feature is a clear NDR behavior even at room temperature in device VB0743. In comparison, this behavior

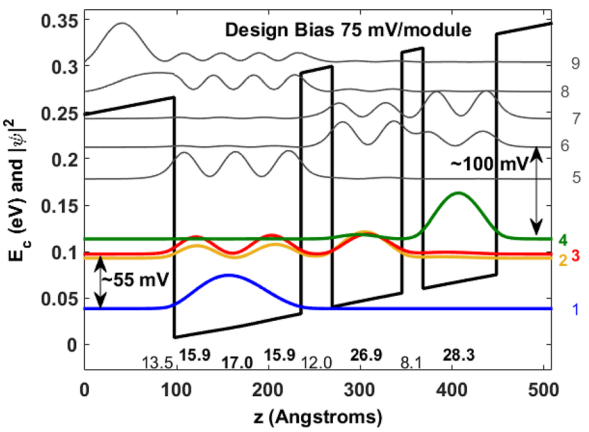


FIG. 4. Band diagram of device VB0743. Arrows mark the intersubband energy spacing between the ULL (level 4) and the first (relevant) excited state (level 6) and the one between the LLL-doublet (levels 2 and 3) and the injector state (level 1). The design bias is ~75 mV/module. For comparison, the HBD design has intersubband separation around ~60 mV between the ULL and the first excited state and ~36 mV between the LLL-doublet and injector state, respectively. Its design bias is ~57 mV/module.

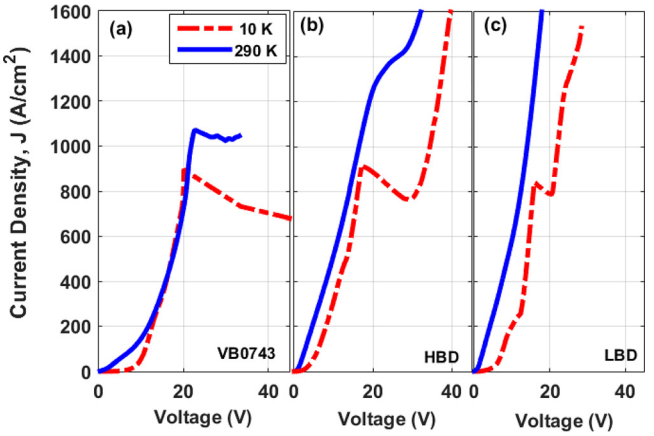


FIG. 5. Measured current–voltage curves at low temperature ~10 K (red dashed-dotted lines) and room temperature ~290 K (blue solid lines) of devices VB0743 (a) HBD (b) and LBD (c).

is not observed in devices LBD and HBD, which show only positive conductance at room temperature. The observation of an NDR behavior at room temperature is a strong evidence of the effective suppression of all the leakage channels in device VB0743. In contrast, various leakage channels dominate the transport at room temperature in both HBD and LBD, and no NDR behavior is observed in either device. This finding validates that the limiting mechanism in the high-barrier device HBD is the thermal excitation of carriers into higher lying levels followed by their relaxation in non-lasing paths. In addition, this result suggests that the excited states must be pushed towards higher energies in order to suppress carrier leakage channels and their effect on the ULL lifetime.

Despite the suppression of the leakage channels, device VB0743 showed a much lower $T_{max}$ than devices HBD and LBD. We attribute this inferior performance to the higher intersubband spacing between the LLL and the injector state in device VB0743 (~55 meV instead of 36 meV), resulting in an increased LO-phonon scattering time (from ~0.23 ps to ~0.91 ps). This results in an increase of the LLL lifetime and likely explains the much higher threshold current density at low temperatures (~725 A/cm$^2$ for device VB0743 compared to ~450 A/cm$^2$ for device HBD, Table II). As a result, the dynamic range of device VB0743 is significantly reduced, so is $T_{max}$. An additional effect that may contribute to the reduced performance of high-barrier devices, including the ones of this work, may be the interface roughness scattering[13–16] which scales up with the increase of the barriers' height. This may result in increased non-radiative scatterings between the lasing states and may promote carrier leakage into higher states.[13–16] However, in contrast to what is observed in this work, an earlier work on tall barrier THz-QCLs shows slightly better laser performance for a device with pure AlAs injector barriers (in comparison to a 15% Al reference device),[5] suggesting a negligible negative contribution of the interface roughness scattering to the device's performance. Clearly, the effects of interface roughness scattering on the performance of high barriers THz-QCLs still need further investigations.

In conclusion, we have studied the temperature degradation of highly diagonal THz-QCLs with high barriers and

identified an additional mechanism that limits their performance which is the excitation of carriers into higher energy states followed by their relaxation in non-lasing paths. Based on this understanding, we have designed a high-barrier THz-QCL with the excited states pushed to higher energies. This new structure showed nonlinear current-voltage curve with negative differential resistance (NDR) behavior all the way up to room temperature. This result indicates a reduced thermally activated excitation of carriers into higher states and suppression of leakage channels. The presence of NDR even at room temperature is encouraging for achieving high-temperature operation of THz-QCLs. Our analysis also points to the direction for further improvement: reducing the lifetime of lower lasing level while eliminating all the thermal leakage channels, including intersubband LO-phonon scatting and thermal activation to both continuum and high-lying states. In such structures, further optimization could be achieved by means of diagonality- and doping-engineering.[17]

The authors would like to thank Yuri V. Flores for helpful discussions and for his help in clarifying this manuscript. A.A. would like to acknowledge the generosity of the MIT-Technion and Andrew and Erna Finci Viterbi Fellowships and their support during this study. This work was supported by NSF and Israel MoD, and also performed at the Center for Integrated Nanotechnologies, a U.S. Department of Energy, Office of Basic Energy Sciences user facility. Sandia National Laboratories is a multi-program laboratory operated by Sandia Corporation, a wholly owned subsidiary of Lockheed Martin Corporation, for the U.S. Department of Energy's National Nuclear Security Administration under Contract No. DE-AC04-94AL85000.

[1]U. S. Fathololoumi, E. Dupont, C. W. I. Chan, Z. R. Wasilewski, S. R. Laframboise, D. Ban, A. Matyas, C. Jirauschek, Q. Hu, and H. C. Liu, Opt. Express **20**(4), 3866 (2012).
[2]S. Kumar, Q. Hu, and J. L. Reno, Appl. Phys. Lett. **94**, 131105 (2009).
[3]A. Albo and Q. Hu, Appl. Phys. Lett. **107**, 241101 (2015).
[4]T. T. Lin, L. Ying, and H. Hirayama, Appl. Phys. Express **5**, 012101 (2012).
[5]C. W. I. Chan, Q. Hu, and J. L. Reno, Appl. Phys. Lett. **103**, 151117 (2013).
[6]L. Schrottke, X. Lü, G. Rozas, K. Biermann, and H. T. Grahn, Appl. Phys. Lett. **108**, 102102 (2016).
[7]A. Albo and Y. V. Flores, "Temperature-driven enhancement of the stimulated emission rate in terahertz quantum cascade lasers," Appl. Phys. Lett. (submitted).
[8]C. W. I. Chan, "Towards room-temperature terahertz quantum cascade lasers: Directions and design," Ph.D. thesis, Massachusetts Institute of Technology, Department of Electrical Engineering and Computer Science, 2015.
[9]Y. V. Flores, M. P. Semtsiv, M. Elagin, G. Monastyrskyi, S. Kurlov, A. Aleksandrova, J. Kischkat, and W. T. Masselink, J. Appl. Phys. **113**, 134506 (2013).
[10]D. Botez, C.-C. Chang, and L. J. Mawst, J. Phys. D: Appl. Phys. **49**, 043001 (2016).
[11]C. Pflügl, L. Diehl, A. Lyakh, Q. J. Wang, R. Maulini, A. Tsekoun, C. K. N. Patel, X. Wang, and F. Capasso, Opt. Express **18**(2), 746–753 (2010).
[12]A. Albo and Q. Hu, Appl. Phys. Lett. **106**, 131108 (2015).
[13]S. G. Razavipour, E. Dupont, Z. R. Wasilewski, and D. Ban, J. Phys.: Conf. Ser. **619**, 012003 (2015).
[14]K. A. Krivas, D. O. Winge, M. Franckié, and A. Wacker, J. Appl. Phys. **118**, 114501 (2015).
[15]M. Franckié, D. O. Winge, J. Wolf, V. Liverini, E. Dupont, V. Trinité, J. Faist, and A. Wacker, Opt. Express **23**, 5201 (2015).
[16]Y. V. Flores, S. S. Kurlov, M. Elagin, M. P. Semtsiv, and W. T. Masselink, Appl. Phys. Lett. **103**, 161102 (2013).
[17]C. W. I. Chan, A. Albo, Q. Hu, and J. L. Reno, "Tradeoffs between oscillator strength and lifetime in terahertz quantum cascade lasers," Appl. Phys. Lett. (submitted).